Ocean Sci. Discuss., https://doi.org/10.5194/os-2017-55
Manuscript under review for journal Ocean Sci.
Discussion started: 27 June 2017

Ocean Science
Discussions
Open Access
EGU

Combining physical and geochemical methods to investigate lower halocline water formation and modification along the Siberian continental slope

Matthew B. Alkire[1], Igor Polyakov[2], Robert Rember[2], Andrey Pnyushkov[2], Vladimir Ivanov[3, 2], Igor Ashik[3]

[1]Applied Physics Laboratory, University of Washington, Seattle, WA USA
[2]International Arctic Research Center, University of Alaska Fairbanks, Fairbanks, AK USA
[3]Arctic and Antarctic Research Institute, St. Petersburg, RUS

Correspondence to: Matthew B. Alkire (malkire@apl.washington.edu)

Abstract. A series of cross-slope transects were occupied in 2013 and 2015 that extended eastward from St. Anna Trough to the Lomonosov Ridge. High-resolution physical and chemical observations collected along these transects revealed fronts in the potential temperature and the stable oxygen isotopic ratio ($\delta^{18}O$) that were observed north of Severnaya Zemlya (SZ). Using linear regressions, we describe mixing regimes on either side of the front that characterize the convective formation of lower halocline water (LHW) and the cold halocline layer. Initial freshening of Atlantic water by sea-ice meltwater occurs west of SZ whereas higher influences of meteoric water and brine result in a transition to a separate mixing regime that alters LHW through mixing with overlying waters and shifts the characteristic temperature-salinity bend from higher ($34.4 \leq S \leq 34.5$) toward lower ($34.2 \leq S \leq 34.3$) salinities. These mixing regimes appear to have been robust since at least 2000.

1 Introduction

The role and relative importance of Atlantic water (AW) heat in shaping the Arctic Ocean's ice cover is still under debate (e.g., Polyakov et al., 2012b). One significant source of uncertainty is the impact of diapycnal fluxes on the cold halocline layer (CHL), which separates the fresh and cold surface mixed layer (SML) from AW (e.g., Aagaard et al. 1981; Pfirman et al. 1994; Schauer et al. 1997; 2002). The stratification of the CHL, representing strong vertical gradients of salinity and density though a negligible gradient of temperature, impedes vertical mixing and upward transport of AW heat (e.g., Rudels et al., 1996; Steele & Boyd, 1998). The base of the CHL represents a transition between the halocline and the reverse thermocline, wherein the temperature increases with depth toward the core of the AW (150-400 m). This transition is known as the LHW, a separate water mass that is commonly identified by a "kink" in the θ-S diagram (see Fig. 1c). The formation of LHW and its modification through diapycnal and/or turbulent mixing with underlying Atlantic water on the Siberian continental slope have important implications for the heat budget and sea ice cover of the Arctic Ocean (e.g., Polyakov et al.,

Ocean Sci. Discuss., https://doi.org/10.5194/os-2017-55
Manuscript under review for journal Ocean Sci.
Discussion started: 27 June 2017

2017). Therefore, it is important to be able to discern between LHW varieties formed by different mechanisms and the modification of these LHW sources through mixing.

Various mechanisms have been proposed for explaining the formation of LHW in the Nansen Basin of the Arctic Ocean. Initially, hypotheses suggested LHW was formed via salinization of Siberian shelf waters through brine rejection and subsequent transport of these waters offshore (i.e., the advective mechanism) (Aagaard et al., 1981; Jones & Anderson, 1986; Steele et al., 1995). At present, it is generally agreed that the primary mechanism of LHW formation results from the modification of AW by melting sea ice upon entry into the Arctic through Fram Strait and the Barents Sea (Rudels et al., 1996; 2004). In this scenario, relatively fresh ($34 \leq S \leq 34.3$) SML water undergoes convective mixing through cooling and brine release during winter sea ice formation. This winter mixed layer (WML) is advected along the Siberian continental margin and is eventually capped by low-salinity shelf waters moving offshore, limiting subsequent convection.

Steele and Boyd (1998) suggested a combined, advective-convective mechanism wherein LHW is formed primarily in the marginal ice zone north of the Barents Sea via convective processes and subsequently interleaves between the WML and AW, forming the CHL through mixing during advection. In contrast, Kikuchi et al. (2004) argued that the initial exposure of AW to freezing conditions upon entry into the Arctic Ocean can be sufficient to restrict any subsequent vertical mixing, such that additional buoyancy flux is unnecessary. Thus, the Kikuchi et al. (2004) hypothesis allows for an entirely convective formation for halocline waters whereas those proposed by Steele & Boyd (1998) and Rudels et al. (1996) imply an advective role from shelf waters.

Rudels et al. (2004) suggested that both mechanisms of halocline formation are possible, resulting in two different sources of halocline water in the eastern Arctic: Fram Strait Branch (FSB) and Barents Sea Branch (BSB) halocline waters. According to Rudels et al. (2004), the FSB branch variety of halocline water is formed via interaction between inflowing AW and sea ice north of Svalbard and subsequent convection in the Nansen Basin, quite similar to the convective LHW mechanism of Rudels et al. (1996). The BSB variety is formed in the Barents Sea through a complex combination of processes resembling the advective-convective mechanism outlined by Steele & Boyd (1998). Rudels et al. (2004) further postulates that after entering the Eurasian Basin through St. Anna Trough (SAT), the BSB halocline water remains close to the Siberian continental slope, and after crossing the Lomonosov Ridge ventilates the lower halocline of the Makarov Basin, between the Mendeleyev Ridge and the Chukchi Cap, as well as the southern Canada Basin. In contrast, the FSB halocline water is displaced farther offshore, ventilating the halocline of the Amundsen and Makarov Basins, as well as northern Canada Basin.

The BSB halocline water has been found to be both thicker and warmer compared to colder and fresher FSB halocline waters. These distinctions can be visually recognized in a θ-S diagram: the cooler FSB variety is expected to exhibit a sharp θ-S kink close to the freezing point (e.g., Fig 1e) whereas the thicker and warmer BSB variety is generally characterized by a smoother kink farther from the freezing point line (e.g., Fig. 1k). Thus, differences can be observed in the properties of halocline waters occupying the slope ("on-slope") versus those located farther offshore ("off-slope").

Ocean Sci. Discuss., https://doi.org/10.5194/os-2017-55
Manuscript under review for journal Ocean Sci.
Discussion started: 27 June 2017

Woodgate et al. (2001) attributed these cross-slope distinctions to differences in the formation processes (i.e., advective vs. convective halocline water). Rudels et al. (2004) attributed these differences to enhanced turbulent mixing between the BSB halocline water and underlying (and warm) AW. They argued that the mixing acts to entrain more AW into the halocline, making it both thicker and warmer while simultaneously cooling the AW layer. Dmitrenko et al. (2011) argued that turbulent vertical mixing occurring locally on the Laptev Sea slope explains the differences observed between warmer/on-slope and cooler/off-slope LHW properties observed along a regularly occupied section (~126 °E) in the Laptev Sea between 2002 and 2009; however, they did not consider the possibility of lateral advection of cross-slope differences from upstream.

Despite the importance of river water and sea-ice melt/brine in LHW formation, few studies have utilized $\delta^{18}O$ to investigate halocline water formation or modification through mixing. It is the purpose of this paper to pair a high density of $\delta^{18}O$ measurements (focused on the halocline layer) with CTD-based temperature and salinity measurements collected along a series of cross-slope transects extending from the SAT to the Lomonosov Ridge to improve our understanding of LHW formation, circulation, and modification through mixing with Siberian shelf waters and underlying AW.

2 Data & methods

In collaboration with the Arctic and Antarctic Research Institute (St. Petersburg, Russia), oceanographic cruises were conducted within the Eurasian Basin and along the slope of the Kara, Laptev, and East Siberian Seas during summers of 2013 (August 23-September 19) and 2015 (August 28-September 26) aboard the research vessels *Akademik Fedorov* and *Akademik Tryoshnikov*, respectively. Totals of 116 (2013) and 94 (2015) hydrographic stations were occupied during the cruises. At all stations, a rosette equipped with 24 Niskin bottles, a Seabird SBE9*plus* CTD (conductivity-temperature-depth), and additional sensors were deployed (further details provided in Supplementary Text S1). At all but 8 (2013) and 6 (2015) stations, water samples were collected for a variety of chemical and biological measurements at routine depths of 500, 250, 200, 150, 140, 130, 120, 110, 100, 90, 80, 70, 60, 50, 40, 30, 20, 10, and 2-4 m (surface).

Samples for $\delta^{18}O$ analyses were collected into 20 mL glass vials, the caps of which were fitted with conical polyethylene inserts, parafilmed, and shipped to the Stable Isotope Laboratory, Oregon State University, for analysis via the CO_2 equilibration method on a Finnegan Mat 251 mass spectrometer. Totals of 1254 and 1940 samples were collected in 2013 and 2015, respectively. Precision was estimated to be ± 0.02 ‰ (2013) and 0.04 ‰ (2015), based on the mean standard deviations of field duplicates. Laboratory duplicates were also conducted to ascertain the performance of the mass spectrometer. Of these, the mean standard deviation was ± 0.02 ‰ during both years. Bottle salinities are not reported due to malfunction of the salinometer available aboard each ship. Instead, CTD properties were matched to bottles via averaging measurements associated with each bottle trip depth using the bottle (.ros) files recorded for each cast. The accuracy of temperature and conductivity measurements recorded by the CTD is expected to be within ± 0.0003 S m^{-1} and ± 0.001C, respectively, per manufacturer specifications. For further details and data access, readers are referred to the NABOS project website (http://research.iarc.uaf.edu/NABOS2/) and/or the NSF Arctic Data Center (https://arcticdata.io).

Ocean Sci. Discuss., https://doi.org/10.5194/os-2017-55
Manuscript under review for journal Ocean Sci.
Discussion started: 27 June 2017

3 Results

Transects occupied during 2013 indicated that the WML, identified as a potential temperature minimum (θ_{min}) below the warmer and fresher SML (Rudels et al., 1996), was associated with salinities > 34. The presence of a seasonal, rather than a permanent, halocline layer was evidenced by higher salinities ($S \geq 34$) at 40-50 m depth (Fig. 2d), potential temperatures near the freezing point at S = 34.1 (e.g., red lines in Fig. 1e), and relatively weak stratification between the base of the WML and the θ-S bend identifying LHW (Fig. 1); thus, a permanent CHL was either very weak or absent throughout most of our study area (Steele and Boyd, 1998; Kikuchi et al., 2004; Bourgain and Gascard, 2011).

At stations in the western part of the study area, it was also apparent that the θ-S kink was sharp, close to the freezing point, and at a relatively shallow depth (typically ≤ 50 m) (Fig. 1d-f) indicating the halocline was convectively formed and likely seasonal (Steele et al., 1995; Rudels et al., 1996; Steele and Boyd, 1998). Farther eastward, the L3 and L4 transects exhibited a front that separated stations closer to shore versus those farther offshore (Fig 1g-h). This front marked a significant change in the core AW temperature (Fig. 2f) as well as a θ increase (Fig. 2e) and $\delta^{18}O$ decrease (Fig. 2c) in the salinity range $34.4 \leq S \leq 34.5$ and an apparent shift of the θ-S bend marking the position of LHW towards lower salinities ($34.2 \leq S \leq 34.3$) (e.g., Fig. 1g). Coincident with this θ-S front, there was also a change in the predominant source of freshwater near the surface. Sea-ice meltwater (SIM) fractions were positive and larger than fractions of meteoric water (MW) along the lengths of sections SAT, L1, and L2 as well as the nearshore stations comprising sections L3 and L4; however, transects L5, L5.5, and L6 all exhibited predominate freshening by MW (Fig. 2a-b). Bauch et al. (2014) reported a similar, zonal gradient along the Siberian slope, with increasing contributions of both MW and brine from west to east, where shelf waters are advected offshore at ~140 °E (in the northeastern Laptev Sea) and contribute to layers overlying LHW ($S \leq 33$).

The easternmost stations of the SAT transect and the southernmost stations of transects L2 and L3 exhibited θ-S characteristics expected for BSB AW (black lines in Fig. 1d, f, g). At L5, three stations inshore of the ~1250 m isobath (< 77.2 °N) exhibited θ-S characteristics (Fig. 1i) synonymous with northern Barents Sea Shelf Water (Woodgate et al., 2001). These observations generally agree with the expectation that BSB waters are restricted to the slope and indicate the predominance of FSB/convective LHW throughout most of the study area. We note that θ-S characteristics of BSB waters were not apparent along transects L1 or L4, possibly indicating that we failed to sample far enough inshore at these transects.

Ocean Sci. Discuss., https://doi.org/10.5194/os-2017-55
Manuscript under review for journal Ocean Sci.
Discussion started: 27 June 2017

4 Discussion

4.1 Geochemical separation of mixing regimes

The coincident shift in freshwater sources was also marked by an obvious break in δ^{18}O-S mixing at $34.4 \leq S \leq 34.5$ (Fig. 3a). The stations occupied along the SAT, L1, L2, and southern portions of the L3 and L4 transects (including those stations exhibiting BSB influence) all exhibited similar mixing regimes in δ^{18}O-S space that indicated predominate freshening by SIM. This group of stations all plotted along the upper linear mixing line of the δ^{18}O-S break. In fact, separate linear regressions from these transects were all statistically indistinguishable (see Supplementary Table S1); thus, a single δ^{18}O-S linear regression was constructed using these data to define the SIM mixing branch for $S \geq 34.5$ (Fig. 3b). Similarly, stations farther offshore on L3 and L4 were combined with the L5 transect to construct the MW mixing branch for $S \geq 34.5$ (Fig. 3c). In addition to the separation of the MW and SIM branches at the δ^{18}O-S break ($34.4 \leq S \leq 34.5$), there was also a clear bend in the δ^{18}O-S relationship at salinities ≤ 34.5 on the MW branch (Fig. 3c). This bend indicates a separate mixing regime that characterizes waters overlying the LHW. A linear regression restricted to the salinity range $34 \leq S < 34.5$ yielded a steeper slope and more negative intercept that indicates higher influences of MW and brine (i.e., negative SIM) typical of Siberian shelf waters (Bauch et al, 2011). In contrast, a similar linear regression of the SIM branch stations in this salinity range returned coefficients that were statistically indistinguishable from the more saline ($S \geq 34.5$) regression (see Supplementary Table S2); thus, the SIM branch extends over the entire water column.

Eastward of ~126 ºE, stations along the L5.5 and L6 transects generally exhibited δ^{18}O values that were somewhat higher/more positive than the mixing line of the lower MW branch (Fig. 3d). Thus, this mixing relationship is altered between the Laptev and East Siberian Seas, perhaps due to a larger influence from positive (or less negative) SIM and/or entrainment of thermocline waters containing a larger influence from AW. Rivers flowing in the East Siberian Sea are typically characterized by more negative δ^{18}O values compared to the Lena, Ob, and Yenisey Rivers (Cooper et al., 2008) so increased MW influence cannot solely explain the more positive δ^{18}O values.

Data collected in the same study area in 2015 suggests a very similar hydrographic setting (i.e., weak/absent CHL with similar cross-slope fronts observed at repeated transects). The salinity-δ^{18}O data generally agree with the scheme proposed here (see Supplementary Tables S4 & S5) as they plot along the three branches characterized using the 2013 data set (Fig. 4a). Furthermore, data collected from different areas of the eastern and central Arctic (specifically the Siberian shelves and the Nansen, Amundsen, and Makarov Basins) also generally plot along the three mixing lines defined in this study (Fig. 4b-d). These data sets also confirm the dominance of the MW branch (and restricted nature of the SIM branch) since all data collected east of ~110 °E (approximate position of the L3 transect) since 2000 returned regression coefficients that were similar to those defined for the MW branch (see Supplementary Table S6).

Ocean Sci. Discuss., https://doi.org/10.5194/os-2017-55
Manuscript under review for journal Ocean Sci.
Discussion started: 27 June 2017

4.2 Interpretation of mixing branches: convection vs. advection

Aksenov et al. (2011) describe the Arctic Shelf Break Branch (ASBB) of the Arctic Circumpolar Boundary Current as a narrow current that transports halocline waters from the Barents and Kara Seas northward via the SAT and eastward along the Siberian continental slope over approximately the 1500 m isobath. Their description is similar to the circulation scheme of advective/BSB LHW proposed by Rudels et al. (2004). More recently, Bauch et al. (2016) used a combination of geochemical tracers collected across the Siberian continental margin between 2005 and 2009 in a principle components analysis to identify four separate LHW types: c1 (S~33), c2 (S~34), c3 (S~34.2), and c4 (S~34.4). Types c2 and c4 were the most commonly observed in the data set, originating at the shelf break north of SZ (type c4) or ~126 °E (type c2) and both extending eastward to at least ~140 °E. Bauch et al. (2016) argued that the regular presence of type c4 LHW north of SZ suggests the Kara Sea as a source of this LHW type. They further postulated that this water leaves the Kara Sea via SAT and/or Voronin Trough and circulates around the slope via the ASBB. Similarly, they argue that type c2 LHW is formed in either the northwestern Laptev Sea or (more likely) in the southeastern Kara Sea and transported to the slope via Vilkitsky Strait.

The description offered by Bauch et al. (2016) for the formation and circulation of LHW types c2 and c4 is also reminiscent of advective/BSB LHW. However, these LHW types are found both on and off the slope, rather than restricted to the continental slope as expected for BSB LHW (Woodgate et al., 2001; Rudels et al., 2004). Bauch et al. (2016) argue that off-slope transport might occur directly or via recirculating waters from the eastern Eurasian Basin (van der Loeff et al., 2012). We observed θ and $\delta^{18}O$ characteristics associated with salinities of 34, 34.2, and 34.4 that are quite similar to the LHW types described by Bauch et al. (2016); however, these similarities were restricted to MW branch stations (all located off slope). In addition, the $\delta^{18}O$ values associated with salinities 34.4-34.5 at SIM branch stations were much higher than those reported by Bauch et al. (2016). These apparent discrepancies suggest different formation and/or circulation schemes compared to those provided by Bauch et al. (2016). Here, we offer an alternative hypothesis.

The WML observed at stations located in the western transects (SAT, L1, and L2) is formed through freshening of AW with SIM and some small contribution of MW to establish a seasonal halocline; these processes produce the SIM branch. However, this branch likely only represents an initial condition as further stratification is necessary to prevent winter mixing from eroding the LHW (and the SIM branch is not observed eastward of SZ). We interpret the transition from SIM to MW branches north of SZ as descriptive of the formation of LHW by convective processes (Rudels et al., 1996). We suggest that this transformation occurs via homogenization of the water column through mixing and salinization from brine expulsion during sea ice formation. To test this hypothesis, we estimated new mixed layer (ML) salinities at the SIM branch stations assuming mixing penetrated to the previous WML depth and then calculated the changes in salinity and $\delta^{18}O$ due to sea ice formation. The mean WML depth and salinity was ~62 m and 34.22, respectively, for all SIM branch stations (see

Ocean Sci. Discuss., https://doi.org/10.5194/os-2017-55
Manuscript under review for journal Ocean Sci.
Discussion started: 27 June 2017

Supplementary Table S3). Mixing of the water columns at individual stations down to their respective WMLs resulted in a new, mean ML salinity of ~33.79 with a corresponding $\delta^{18}O$ value of ~0 ‰ (calculated using the SIM branch regression). Brine expulsion from 1.0-1.5 m of sea ice growth increases the salinity to between 34.25 and 34.48 and decreases $\delta^{18}O$ to between -0.05 and -0.07 ‰. These resulting salinity and $\delta^{18}O$ values roughly plot along the upper or lower MW branches (Fig. 3e & Supplementary Figure S1). Continued influence from Siberian shelf waters results in the steeper slope and highly negative intercept of the lower MW branch and isolates the LHW from subsequent surface mixing; this process also forms the CHL.

While mixing down to the previous year's WML (or shallower) might be expected given the increase in freshwater inventories (and stratification) moving from west to east along the slope, deeper mixing was observed in the study region between 2013 and 2015 (Polyakov et al., 2017). The depth of the 34.4 isohaline ranged between 60 and 100 m at the MW branch stations. If we consider mixing down to 100 m and 1 m of ice formation, the resulting salinity (34.50) and $\delta^{18}O$ (0.07 ‰) resemble the upper MW branch at the break point. Thus, both shallower (~60 m) and deeper (~100 m) mixing result in a transition to the MW branch. Although mixing and brine release can account for salinity and $\delta^{18}O$ changes, additional mixing (either lateral or vertical) with warm AW is needed to produce $\theta \approx -1$ °C associated with the LHW of the MW branch. A mixture comprising ~75 % of newly formed MW branch water (34.25, -0.05 ‰, and -1.88 °C) and ~25 % AW (34.9, 0.3 ‰, and 2 °C) would produce the observed salinity (34.4), θ (-0.91 °C), and $\delta^{18}O$ (0 ‰) observed.

It is also important to note that MW must have been supplied to the region north of SZ to define the front separating SIM and MW branches. We adopt the suggestion made by Bauch et al. (2016) that waters moving off the shelf in the northeastern Laptev Sea (i.e., along the Lomonosov Ridge) are recirculated westward, except we suggest this recirculation does not necessarily extend to halocline waters but instead only to near surface waters containing MW and brine. In support of this hypothesis, we note that the salinity and $\delta^{18}O$ values characterizing the four LHW types defined by Bauch et al. (2016) form a salinity-$\delta^{18}O$ mixing line ($\delta^{18}O = 0.9828S - 33.901$) similar to the lower MW branch identified in this study (Supplementary Figure S2). This could indicate that the four LHW types described by Bauch et al. (2016) are actually mixtures of convectively formed LHW and increasing contributions of MW progressing eastward from SZ.

5 Summary & conclusions

A cross-shore front was observed north of SZ at sections L3 and L4 that separated mixing branches dominated by either SIM (inshore) or MW (offshore). Both LHW (S~34.4) and the θ_{max} marking the AW core were relatively cooler at stations inshore of the front. Upstream at transects L1 and L2, colder halocline waters originating from the Barents Sea were generally found at stations inshore of the ~1600 m isobath (in agreement with Aksenov et al., 2011) whereas those farther offshore were either clearly dominated by warmer, FSB AW or exhibited mixing between the warmer FSB and colder BSB waters; however, no such fronts occurred in $\delta^{18}O$-S (all stations plotted along the SIM branch). Downstream at the L5

section, three stations inshore of the ~1250 m isobath (< 77.2 °N) exhibited BSB-like θ-S characteristics but anomalously low $\delta^{18}O$ values (≤ -0.2 ‰) between salinities 34.4 and 34.7 indicating large contributions of brine. All other stations on L5 plotted along the MW branch. Thus, if BSB LHW was advected within the ASBB, it was restricted to the shallowest depths encountered during the 2013 and 2015 cruises and likely undergoes additional modification through interaction with shelf waters. Farther east at transects L5.5 and L6, stations generally plotted along the MW branch but exhibited signs of additional modification.

We interpret these observations as indicative of two stages of mixing that contribute to the formation of convective LHW. The first stage is described by the SIM branch as AW is freshened predominately by ice melt and is then subject to further modification through subsequent vertical mixing (with less saline, overlying waters) and ice formation. The vertical mixing reduces both salinity and $\delta^{18}O$ of the WML and ice formation then increases the salinity but only slightly decreases the $\delta^{18}O$. This process results in a shift from the SIM branch to the MW branch north of SZ and causes a prominent break in salinity-$\delta^{18}O$ space in the salinity range $34.4 \leq S \leq 34.5$. The second stage is described by mixing with Siberian shelf waters containing large influences from MW and brine (negative SIM), resulting in a bend in the $\delta^{18}O$-salinity relation and isolates the LHW from surface processes. Comparisons against other data sets collected between 2000 and 2015 suggest that the salinity-$\delta^{18}O$ mixing regimes defined here remain relatively stable despite changes to the sea ice cover (Polyakov et al., 2017), the temperature and volume of AW inflow (e.g., Polyakov et al., 2012a), and distribution of river runoff (Guay et al., 2001; Dmitrenko et al., 2005). Instead, we speculate that such changes might alter the front(s) marking the transition between the SIM and MW branches. A comparison of these results with recent studies raises questions as to whether the LHW types identified by Bauch et al. (2016) are independent, advective sources of LHW or products of mixing between convectively formed LHW and less saline shelf waters. Additional observations are necessary to further address these distinctions.

Data availability

All data presented and/or described in this manuscript can be accessed via the National Science Foundation Arctic Data Center (https://arcticdata.io) via the following six data and metadata sets:

Igor Polyakov. 2016. NABOS - CTD Survey Data 2013. Arctic Data Center. doi:10.18739/A2M37F.

Igor Polyakov. 2016. NABOS - Water Quality and Physical Oceanography Data from the Eastern Eurasian and Makarov Basins, and Northern Laptev and East Siberian Seas in 2013. Arctic Data Center. doi:10.18739/A2G95H.

Igor Polyakov. 2016. NABOS - Chemistry Data 2013. Arctic Data Center. doi:10.18739/A2QS91.

Igor Polyakov. 2016. NABOS II - Water Quality and Physical Oceanography Data from the Eastern Eurasian and Makarov Basins, and Northern Laptev and East Siberian Seas in 2013 - 2015. Arctic Data Center. doi:10.18739/A20955.

Igor Polyakov. 2016. NABOS II - CTD Survey Data 2015. Arctic Data Center. doi:10.18739/A2436Q.

Igor Polyakov. 2016. NABOS II - Chemistry Data 2015. Arctic Data Center. doi:10.18739/A27S9P.

Competing interests

The authors declare that they have no competing interests

Acknowledgements

Alkire acknowledges funding from the National Science Foundation (PLR-1203146 AM003) and the National Oceanic & Atmospheric Administration (NA15OAR4310156). Alkire would also like to thank Dr.'s Michael Steele and Rebecca Woodgate (Applied Physics Laboratory) for helpful comments and suggestions during the preparation of this manuscript as well as Wendy Ermold for help in figure preparation. Ivanov acknowledges funding from the Ministry of Education and Science of the Russian Federation (project RFMEFI61617X0076).

References

Aagaard, K., L. K. Coachman, and E. C. Carmack: On the pycnocline of the Arctic Ocean, Deep-Sea Research, 28, 529-545, 1981.

Alkire, M.B., Morison, J., and Andersen, R.: Variability and trends in the meteoric water, sea-ice melt, and Pacific water contributions to the central Arctic Ocean, 2000-2013, Journal of Geophysical Research, 120, 1573-1598, 2015.

Aksenov, Y., V.V. Ivanov, A.J. George Nurser, S. Bacon, I.V. Polyakov, A.C. Coward, A.C. Naveira Garabato, and A. Beszczynska Moeller: The Arctic Circumpolar Boundary Current, Journal of Geophysical Research, 116, C09017, doi:10.1029/2010JC006637, 2011.

Bauch, D. R. van der Loeff, M. Michiel, N. Andersen, S. Torres-Valdes, K. Bakker, and E.P. Abrahamsen: Origin of freshwater and polynya water in the Arctic Ocean halocline in summer 2007, Progress in Oceanography, 91(4), 482-495, doi:10.1016/j.pocean.2011.07.017, 2011.

Bauch, D., S. Torres-Valdes, I. Polyakov, A. Novikhin, I. Dmitrenko, J. McKay, and A. Mix: Halocline water modification and along-slope advection at the Laptev Sea continental margin, Ocean Science, 10, 141-154, 2014.

Bauch, D., E. Cherniavskaia, and L. Timokhov: Shelf basin exchange along the Siberian continental margin: modification of Atlantic Water and Lower Halocline Water, Deep-Sea Research I, 115, 188-198, 2016.

Bourgain, P., and J. C. Gascard: The Arctic Ocean halocline and its interannual variability from 1997 to 2008, Deep-Sea Research I, 58, 745–756, doi:10.1016/j.dsr.2011.05.001, 2011.

Cooper, L. W., McClelland, J. W., Holmes, R. M., Raymond, P. A., Gibson, J. J., Guay, C. K., and Peterson, B. J.: Flow-weighted values of runoff tracers (d18O, DOC, Ba, alkalinity) from the six largest Arctic rivers, Geophysical Research Letters, 35, doi:10.1029/2008GL035007, 2008.

Dmitrenko, I., S. Kirillov, H. Eicken, and N. Markova: Wind-driven summer surface hydrography of the eastern Siberian shelf. Geophysical Research Letters, 32, doi:10.1029/2005GL023022, 2005.

Dmitrenko, I. A., Ivanov, V. V., Kirillov, S. A., Vinogradova, E. L., Torres‐Valdes, S., and D. Bauch: Properties of the Atlantic derived halocline waters over the Laptev Sea continental margin: Evidence from 2002 to 2009, Journal of Geophysical Research, 116, C10024, doi:10.1029/2011JC007269, 2011.

Guay, C.K., K.K Falkner, R.D. Muench, M. Mensch, M. Frank, and R. Bayer: Wind-driven transport pathways for Eurasian Arctic river discharge, Journal of Geophysical Research, 106, 11469-11480, 2011.

Janout, M.A., Y. Aksenov, J.A. Hölemann, B. Rabe, U. Schauer, I.V. Polyakov, S. Bacon, A.C. Coward, M. Karcher, Y.-D. Lenn, H. Kssens, and L. Timokhov: Kara Sea freshwater transport through Vilkitsky Strait: variability, forcing, and further pathywas toward the western Arctic Ocean from a model and observations, Journal of Geophysical Research, 120, 4925-4944, doi:10.1002/2014JC010635, 2015.

Jones, E. P. and Anderson, L. G.: On the origin of the chemical properties of the Arctic Ocean halocline, Journal of Geophysical Research, 91, 10759-10767, 1986.

Kikuchi, T., Hatakeyama, K., and Morison, J.: Distribution of convective Lower Halocline Water in the eastern Arctic Ocean, Journal of Geophysical Research, 109, doi:10.1029/2003JC002223, 2004.

Pfirman, S. L., Bauch, D., and Gammelsrod, T.: The northern Barents Sea: Water mass distribution and modification, In: Johannessen, O.M., R. D. Muench, and J. E. Overland (Eds.), The Polar Oceans and Their Role in Shaping the Global Environment: The Nansen Centennial Volume, Geophys. Monogr. Ser., vol. 85, pp. 77-94, AGU, Washington, D.C., 1994.

Polyakov, I. V., Pnyushkov, A. V., and Timokhov, L. A.: Warming of the intermediate Atlantic Water of the Arctic Ocean in the 2000s, Journal of Climate, 25(23), 8362–8370, DOI 10.1175/JCLI-D-12-00266.1, 2012a.

Polyakov, I. V., Kwok, R., and Walsh, J. E.: Recent changes of arctic multiyear sea-ice coverage and their likely causes, Bulletin of American Meteorological Society, 93(2), 145–151, DOI:10.1175/BAMS-D-11-00070.1, 2012b.

Polyakov, I.V., A.V. Pnyushkov, M.B. Alkire, I.M. Ashik, T.M. Baumann, E.C. Carmack, I. Goszczko, J. Guthrie, V.V. Ivanov, T. Kanzow, R. Krishfield, R. Kwok, A. Sundfjord, J. Morison, R. Rember, and A. Yulin: Greater role for Atlantic inflows on sea-ice loss in the Eurasian Basin of the Arctic Ocean, Science, doi:10.1126/science.aai8204, 2017.

Rudels, B., Jones, E. P., Anderson, L. G., and Kattner, G.: On the intermediate depth waters of the Arctic Ocean, In: The Polar Oceans and Their Role in Shaping the Global Environment: The Nansen Centennial Volume, Johannessen, O.M., R. D. Muench, and J. E. Overland (Eds.), AGU Geophysical Monograph vol. 85, American Geophysical Union, Washington DC, 33-46, 1994.

Rudels, B., Anderson, L. G., and Jones, E. P.: Formation and evolution of the surface mixed layer and halocline of the Arctic Ocean, Journal of Geophysical Research, 101, 8807-8821, 1996.

Rudels, B., Jones, P., Schauer, U., and Eriksson, P.: Atlantic sources of the Arctic Ocean surface and halocline waters, Polar Research, 23(2), 181–208, 2004.

Schauer, U., Muench, R.D., Rudels, B., Timokhov, L.: Impact of eastern Arctic shelf waters on the Nansen Basin intermediate layers, Journal of Geophysical Research, 102(2), 3371-3382, 1997.

Schauer, U., Loeng, H., Rudels, B., Ozhigin, V.K., and Dieck, W.: Atlantic water flow through the Barents and Kara Seas, Deep-Sea Research I, 49, 2281-2298, 2002.

Schlitzer, R.: Ocean Data View. http://odv.awi.de, 2016.

Schmidt, G.A., G. R. Bigg and E. J. Rohling: Global Seawater Oxygen-18 Database - v1.21. https://data.giss.nasa.gov/o18data/, 1999.

Steele, M., Morison, J. H., and Curtin, T. B.: Halocline water formation in the Barents Sea, Journal of Geophysical Research, 100, 881-894, 1995.

Steele, M., and Boyd, T.: Retreat of the cold halocline layer in the Arctic Ocean, Journal of Geophysical Research, 103, 10 419–10 435, 1998.

van der Loeff, M. R., P. Cai, I. Stimac, D. Bauch, C. Hanfland, T. Roeske, and S. B Moran: Shelf-basin exchange times of Arctic surface waters estimated from ^{228}Th/^{228}Ra disequilibrium, Journal of Geophysical Research, 117(C03024), doi:10.1029/2011JC007478, 2012.

Woodgate, R. A., Aagaard, K., Muench, R. D., Gunn, J., Bjork, G., Rudels, B., Roach, A. T., Schauer, U.: The Arctic Ocean boundary current along the Eurasian slope and the adjacent Lomonosov Ridge: water mass properties, transports and transformations from moored instruments, Deep-Sea Research I, 48, 1757-1792, 2001.

Ocean Sci. Discuss., https://doi.org/10.5194/os-2017-55
Manuscript under review for journal Ocean Sci.
Discussion started: 27 June 2017

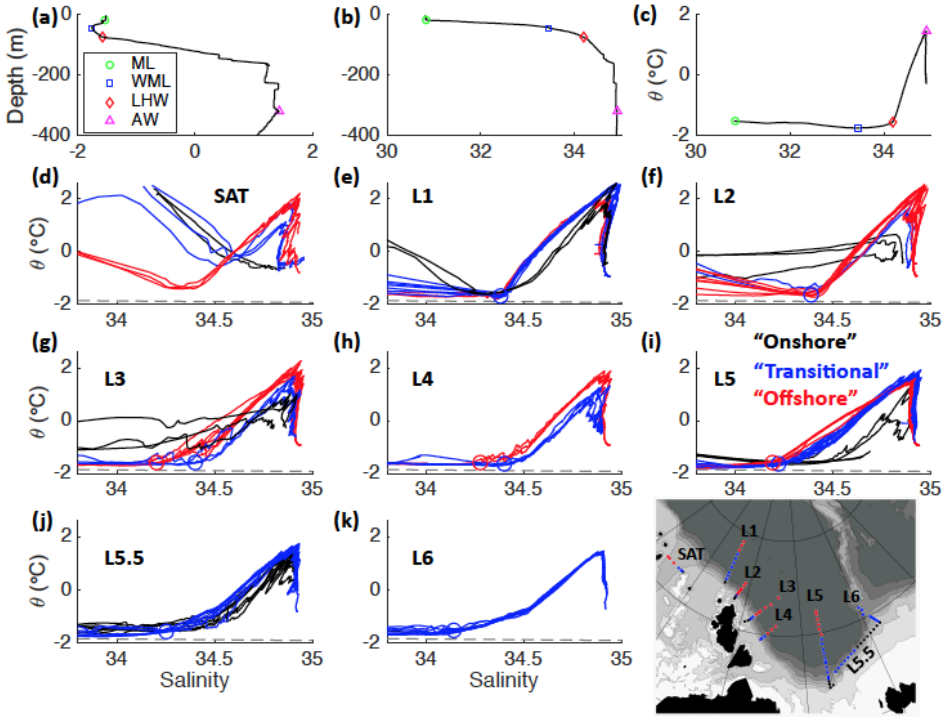

Figure 1. The top three panels illustrate vertical profiles of (a) potential temperature (θ) and (b) salinity, as well as the corresponding θ-S diagram (c) for a single station (station 26) occupied in 2013. The colored symbols show the position of the seasonal mixed layer (ML; green circle), winter mixed layer (WML; blue square), θ-S bend (or "kink") indicating the position of lower halocline water (LHW; red diamond), and the θ_{max} of the core Atlantic water (AW; magenta triangle). The cold halocline is the layer between the WML and LHW. The reverse thermocline is the layer between the LHW and AW. The WML depth was determined as the θ_{min} below the seasonal ML. The LHW position was computed via the method outlined in Bourgain and Gascard (2011). The remaining panels exhibit θ-S diagrams for all data collected during the 2013 cruise. Data are divided among subpanels according to transect (SAT, L1, L2, L3, L4, L5, L5.5, and L6) with the locations of each transect shown in the inset map. The θ-S data measured at each station are colored black (closest to shore or "onshore"), blue ("transitional" between onshore and offshore), or red (farthest "offshore") according to its relative onshore vs. offshore position. Along the St. Anna Trough (SAT) section, the colors indicate the relative position of stations farthest west (red), central/east (blue), and farthest east/shallow (black) rather than onshore/offshore. The relative positions were defined differently along each transect according to fronts observed in θ-S characteristics as described in the text. Red and blue circles on these diagrams show the mean positions of LHW at the transitional and offshore stations along each transect, respectively. LHW positions along L1 and L2 did not significantly differ between transitional and offshore stations; therefore, only a single position is plotted. Note that all stations on the L6 transect were plotted in blue as there was little difference among stations indicative of a θ-S front.

Ocean Sci. Discuss., https://doi.org/10.5194/os-2017-55
Manuscript under review for journal Ocean Sci.
Discussion started: 27 June 2017

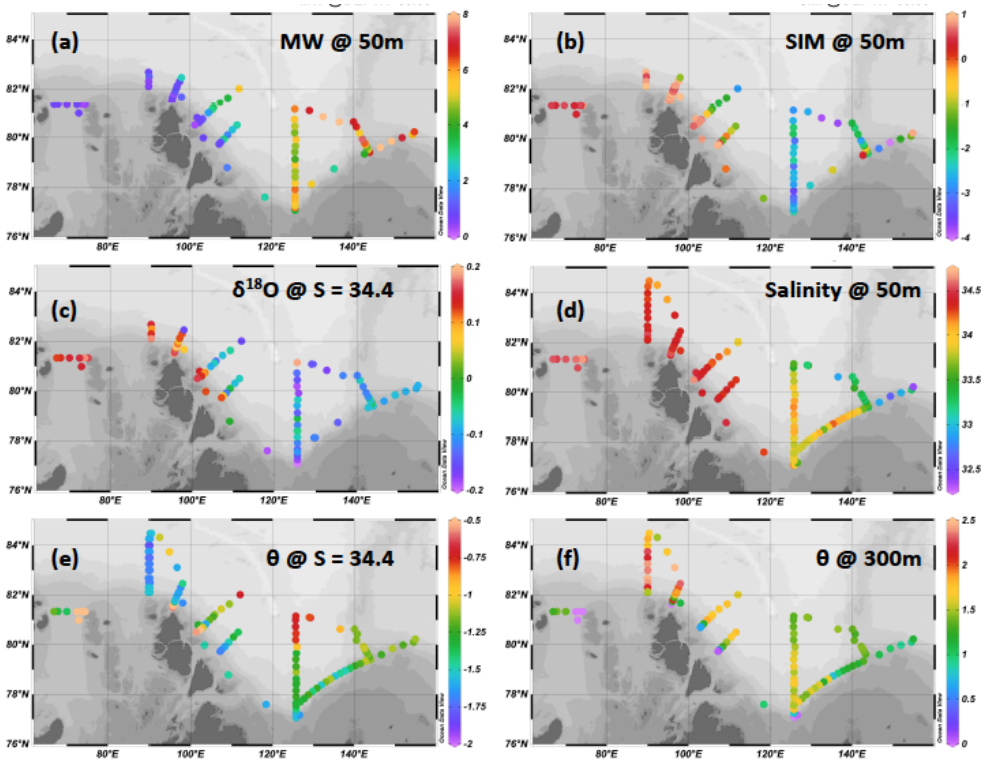

Figure 2. Maps of the (a) meteoric water (MW) fraction (%) at 50 m depth, (b) net sea-ice meltwater (SIM) fraction (%) at 50 m depth, (c) $\delta^{18}O$ (‰) on the 34.4 isohaline, (d) salinity at 50 m depth, (e) potential temperature (°C) on the 34.4 isohaline, and (f) potential temperature (°C) at 300 m (i.e., the approximate depth of the Atlantic water core). The MW and SIM fractions were calculated using a coupled water type analysis conserving salinity, $\delta^{18}O$, and mass according to methods outlined in Alkire et al. (2015); specific details regarding the methods of the analyses are provided in the Supplementary Text S2. Maps were created using Ocean Data View software (version 4.7.6) (Schlitzer, 2016).

Ocean Sci. Discuss., https://doi.org/10.5194/os-2017-55
Manuscript under review for journal Ocean Sci.
Discussion started: 27 June 2017

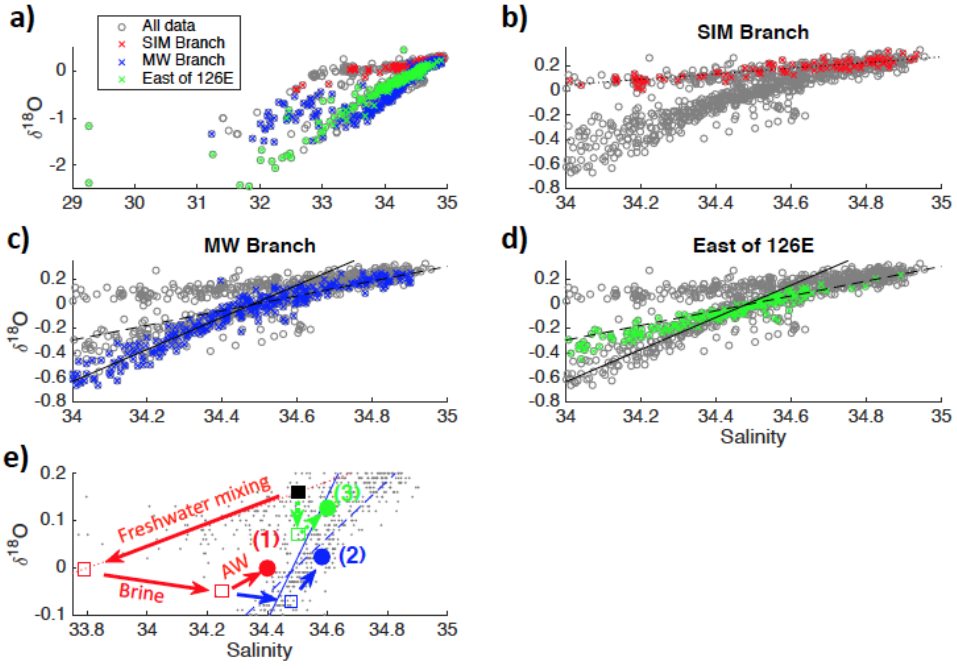

Figure 3. Plots of salinity versus the stable oxygen isotopic ratio ($\delta^{18}O$) measured during the 2013 cruise. The entire data set is plotted in each panel as gray circles. Data collected from stations comprising the sea-ice meltwater (SIM) branch, meteoric water (MW) branch, and remaining stations located east of the L5 transect (L5.5 and L6 transects) are plotted as red, blue, and green x's in panels (b), (c), and (d), respectively. Linear regressions characterizing the SIM ($\delta^{18}O = 0.2287*S - 7.7306$; $R^2 = 0.44$) and MW ($\delta^{18}O = 0.6016*S - 20.7517$; $R^2 = 0.69$) branches ($S \geq 34.5$) are plotted as dotted and dashed lines, respectively. The lower MW branch ($34 \leq S < 34.5$) is plotted as a solid line ($\delta^{18}O = 1.3126*S - 45.2639$; $R^2 = 0.89$). Both MW branches are plotted in panel (d) for comparison against data along L5.5 and L6 transects. Note that the inclusion of all data collected east of 126°E results in a linear regression that was statistically indistinguishable from the MW branch ($\delta^{18}O = 0.63S - 21.8$; $R^2 = 0.71$); however, this was not the case for the lower salinity range; thus, these stations were excluded in the definition of the MW branches. Panel (e) illustrates the transition from the SIM branch to the MW branch via mixing with overlying freshwaters, salinization through sea ice formation/brine release, and mixing with Atlantic waters (AW). The red pathway illustrates the effect of vertical mixing down to ~60 m (the mean winter mixed layer depth at SIM branch stations), brine expulsion due to the formation of 1 m of sea ice, and mixing with AW in a 25:75 ratio to form lower halocline water with a salinity of 34.4 and $\delta^{18}O$ of 0 ‰ (1). The blue pathway deviates from the red pathway due to additional ice formation (1.5 m instead of 1 m) to form lower halocline water with a salinity of 34.58 and $\delta^{18}O$ of 0.02 ‰ (2). The green pathway illustrates the effect of vertical mixing to 100 m, 1 m of sea ice formation, and AW mixing to form lower halocline water with a salinity of 34.6 and $\delta^{18}O$ of 0.13 ‰ (3). Empty squares indicate transition points after each step whereas filled circles indicate the final halocline water product formed by the three potential pathways. All three pathways yield salinity and $\delta^{18}O$ combinations near (but not directly on) the MW mixing branches, indicating some additional processes and/or mixing (such as freshwater influence from river runoff) takes place during the transition from the SIM branch to the MW branch. A larger version of this figure is available in the Supplementary Information, Figure S1.

Ocean Sci. Discuss., https://doi.org/10.5194/os-2017-55
Manuscript under review for journal Ocean Sci.
Discussion started: 27 June 2017

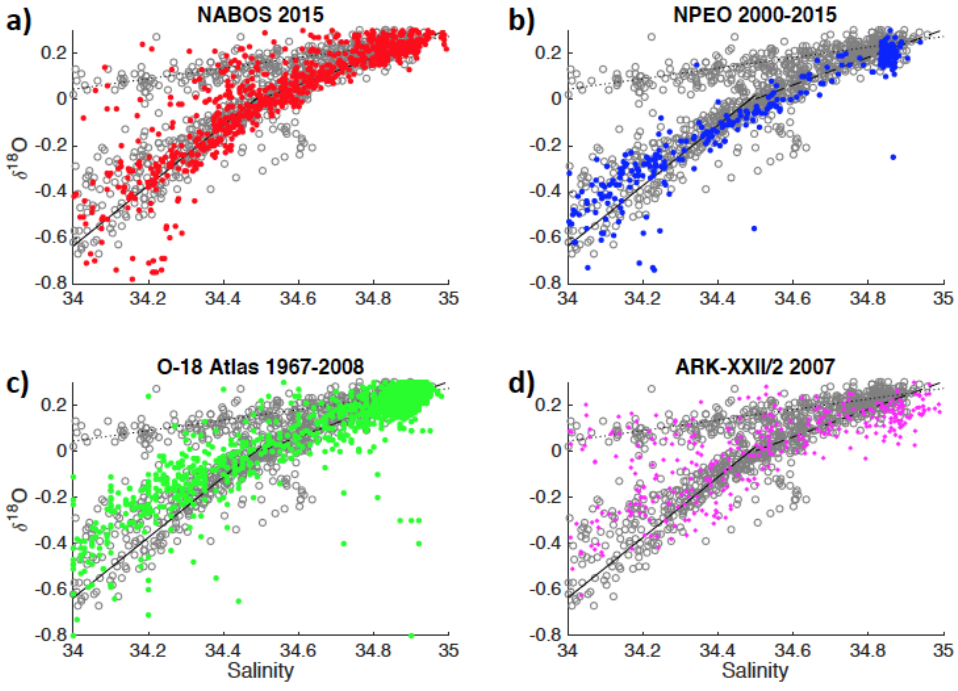

Figure 4. Comparison of data and linear regressions defining the SIM, MW, and lower MW branches defined during the 2013 cruise against additional data sets collected within the study region and in the deep basins of the eastern Arctic (Nansen, Amundsen, and/or Makarov Basins): (a) 2015 cruise; (b) North Pole Environmental Observatory (NPEO); (c) Oxygen-18 Database; and (d) ARK-XXII/2 expedition. In each panel, the 2013 data are plotted as gray circles and the linear regressions are plotted as dotted (SIM Branch), dashed (MW Branch), and solid (lower MW branch) lines. Data from each of the four cruises are plotted as (a) red, (b) blue, (c) green, and (d) magenta dots to indicate the general correspondence of these data with the mixing regimes defined by the three branches. The NPEO data was previously published by Alkire et al. (2015) and can be accessed online at the NSF Arctic Data Center (https://arcticdata.io). The 2015 NABOS cruise data can be accessed online at the NSF Arctic Data Center. Data from the Oxygen-18 Database (Schmidt et al., 1999) were restricted to longitudes 65-160 °E and latitudes 75-90 °N to closely resemble the area sampled for this study. The data can be accessed online at https://data.giss.nasa.gov/o18data/. Data from the ARK-XXII/2 cruise aboard the *Polarstern* were published by Bauch et al. (2011) and can be accessed online via PANGEA (doi:10.1594/PANGAEA.763451).